JOURNAL OF MATERIALS SCIENCE 30 (1995) 4726–4736

Influence of spray atomization and deposition processing on microstructure and mechanical behaviour of an aluminium alloy metal-matrix composite

S. PING YAN, F. A. MOHAMED, E. J. LAVERNIA
Materials Science and Engineering, Department of Mechanical and Aerospace Engineering, University of California, Irvine, CA 92717, USA

T. S. SRIVATSAN
Department of Mechanical Engineering, The University of Akron, Akron, Ohio 44325, USA

An aluminium alloy metal matrix discontinuously reinforced with silicon carbide particulates, was synthesized using the spray atomization and co-deposition technique. Microstructural characterization studies were performed to provide an understanding of the intrinsic effects of carbide particulate co-injection into the aluminium alloy metal matrix. Results reveal the ageing kinetics to be altered by the reinforcing ceramic particulates. Ambient temperature tensile tests revealed that the presence of particulate reinforcement in the aluminium alloy metal matrix degrades both strength and ductility. The results obtained are discussed in relation to thermal conditions during spray co-deposition and contributions from reinforcement to intrinsic microstructural effects and mechanical response.

1. Introduction

Continuous attempts have been made, in the last decade, particularly in areas spanning alloy development and the use of novel processing techniques, to develop high-performance hybrid materials or composites as competitors to the traditional engineering alloys. In particular, much attention has been given to the development of reinforced metallic materials that can offer significant improvements in structural efficiency, reliability, and mechanical performance over the monolithic counterpart. The term metal-matrix composite (MMC) refers to a family of metal-based composite materials reinforced with either continuous or discontinuous reinforcements, to provide an enhanced combination of properties. The matrix material of a metal-matrix composite can be any pure metal or alloy, but most interest is in those metals which find use in structural applications where stiffness and light weight are primary considerations. Thus, the matrices are usually aluminium, titanium or magnesium.

The reinforcement or filler material in currently available metal-matrix composites is normally some form of ceramic, but can be anything other than the matrix metal. The most commonly used fillers are silicon carbide (SiC), boron carbide (BC), aluminium oxide (Al_2O_3) and carbon. The filler takes many forms, ranging from continuous fibres to fine particulates and including discontinuous fibres, whiskers and platelets. The advantages of particulate-reinforced aluminium alloys are manifold. Increases in modulus of greater than 100% have been reported in aluminium alloys reinforced with 40 vol % silicon carbide [1]. Associated with improvements in modulus are concurrent increases in proof strength and ultimate strength of up to 60% [2, 3]. The modulus thus obtained is greater than those of typical titanium alloys and only marginally less than those of most steels. Other reported advantages of the discontinuously reinforced aluminium (DRA) alloy composites over their unreinforced counterparts include a potential for high abrasion resistance [4], improved fatigue crack growth resistance [5, 6], improved fatigue crack initiation resistance [7], increased elevated temperature strength [8], improved creep rupture properties [9], and good micro-creep performance [10]. Furthermore, the particulate-reinforced metal-matrix composites are attractive because they exhibit near isotropic properties when compared to the continuously reinforced counterpart [11–16], besides providing the additional advantage of being machinable and workable [17]. The combination of properties offered by aluminium alloy–silicon carbide particulate MMCs shows potential for applications in the automotive, aerospace, defence and leisure-related industries. The primary disadvantage of the Al/SiC_p, however, is that they suffer from ductility and inadequate fracture toughness when compared to that of the constituent matrix material [18–20].

There are six basic production routes for manufacturing particulate-reinforced aluminium MMCs. These include (i) powder blending, (ii) mechanical alloying, (iii) melt stirring, (iv) compo-casting, (v)

0022–2461

reaction techniques (e.g. Martin Marietta's XD™ technique), and (vi) spray co-deposition. The powder blending technique suffered from the disadvantages of surface-area oxidation of the alloyed powder, especially for the alloy systems of magnesium, aluminium and titanium, coupled with being a fairly expensive process. Also, the blending step is a time consuming, expensive and dangerous operation. Consequently, many interesting possibilities which are feasible through using rapidly solidified powder have to be discarded. The mechanically alloyed product required consolidation and processing in a similar way to materials produced by the powder route, and therefore suffered from the same problems. Melt stirring is limited to those alloys and compositions that can be cast in a non-composite form. Also, the technique suffers from (i) an inability to completely wet the particulate and distribute it evenly in the melt, and (ii) undesirable reactions between the particulate and the melt because of the long-term-high-temperature exposure during processing.

The exothermic dispersion process, commercially designated as the XD technique, was originally developed at the Martin Marietta Laboratories (Baltimore, MD) for the manufacture of composite materials containing finely dispersed ceramic or intermetallic particles in either metallic or intermetallic matrices [21–27]. As described by Westwood [22]; in this process, elemental powders of a high-temperature phase, X and Y (e.g. titanium and boron) are heated in the presence of a third metallic phase, Z (e.g. aluminium), which is typically the matrix alloy. The matrix metal, Z, acts as a solvent and usually melts at a temperature that is well within the requirement to form the stable ceramic phase, XY (e.g. TiB_2). The component elements X and Y then react exothermically, and form micrometre-sized particles in the solvent matrix. Because the dispersoids are formed during *in situ* reactions, it is possible to produce clean matrix/reinforcement interfaces that are totally free from extraneous contaminants. Moreover, it is possible to obtain very large amounts (greater than 40%) of relatively well-dispersed particles, with resultant improvement in strength stiffness and thermal stability [21].

This leaves spray atomization and co-deposition as a novel synthesis technique for the processing of discontinuously reinforced aluminium-base metal-matrix composites [28–39]. This processing technique offers the unique opportunity to synergize the benefits associated with fine particulate technology, that is, refinements in intrinsic microstructural features, modifications in alloy composition, etc., coupled with *in situ* processing and, in some cases, near-net shape manufacturing. The technique also helps in minimizing the deleterious effects associated with oxidation. Precise details of the processing technique, injection details, analysis and results are provided elsewhere [29–34]. A unique feature of this technique is that it avoids the extreme thermal excursions with concomitant degradation in interfacial properties, and extensive macrosegregation associated with conventional casting processes. Furthermore, this novel processing technique avoids extensive, time-consuming and potentially dangerous steps, and eliminates the need for clean powder-handling practices to avoid potentially deleterious pick-up of inclusions. The versatility of the system is demonstrated by an ability to spray such diverse matrices as commercially pure aluminium, and the family of aluminium alloys including aluminium–lithium alloys [39–41]. The final quality of the spray co-deposited MMC is critically dependent on the composition of the matrix alloy chosen.

The objective of this work was to provide an insight into the microstructure, ageing kinetics and tensile behaviour of a spray-atomized and co-deposited aluminium alloy reinforced with fine silicon carbide particulates (SiC_p). The intrinsic microstructural features of the spray-processed MMC are characterized and discussed in relation to alloy composition and processing variables. The room-temperature mechanical properties of the composite are compared with the unreinforced matrix material to highlight the influence of particulate reinforcement, and correlations made with intrinsic microstructural features.

2. Experimental procedure

The material (master alloy) used in this study was provided by the US Army Materials Technology Laboratory (AMTL) at Watertown, MA, in the form of rolled plate of thickness 50 mm. The as-received material was inspected for defects and chemically analysed prior to atomization. The nominal composition (wt %) of the master alloy designated by the Aluminum Association as 2519, is given in Table I. Silicon carbide particulate (α-phase) was the reinforcement used. The size distribution of the silicon carbide particulates was Gaussian with an average particulate size of 3 μm (d_{50}). The density of the SiC_p is 3.1 g cm^{-3} and the surface area of the SiC_p is 8.3 m^2 g^{-1} [41]. A schematic illustration of the spray atomization and co-deposition facility used in this study is shown in Fig. 1. A comprehensive description of the experimental apparatus, the processing procedure and processing variables used can be found elsewhere [29–34, 41–44]. A total of three experiments was conducted. The primary experimental variables used in these experiments are summarized in Table II.

The spray deposit (i.e. the preform) was machined into a billet of diameter 25 mm. The high-density billet was then extruded under a pressure of 55 MPa at a temperature of 450 °C with an area reduction ratio of 16:1. Following hot extrusion, the samples were isochronally heated to 530 °C for 30 min and subsequently quenched in cold water. The as-spray deposited, extruded and solution heated material was aged at 163 °C for various time intervals ranging from 2 h–49 h.

Samples for light optical microscopy were taken from the central section of the spray-processed material. The samples were wet ground on silicon carbide paper using water as lubricant and then mechanically polished using an alumina-based polishing compound. Grain morphology and particulate distribution were revealed using Kroll's reagent as the etchant. The etched samples were observed in an optical

TABLE I Experimental variables

	Variables		
	1	2	3
Atomization pressure (p.s.i.)	176	165	165
Atomization gas	N_2	N_2	N_2
Metal mass flow rate ($g\,s^{-1}$)	32	29	31
Puring temperature (°C)	800	800	800
Flying distance (m)	0.41	0.41	0.41
Injector location (m)	0.19		0.19
Injection gas	N_2	N_2	N_2
Injecting pressure (MPa)	0.17	0.17	0.17

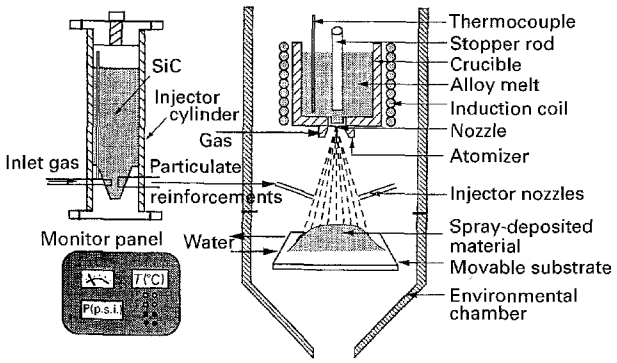

Figure 1 A schematic illustration of the experimental apparatus showing the spray atomization and deposition apparatus.

TABLE II Analysis results of as-deposited materials

	Grain size (μm)	(vol %)	Density ($g\,cm^{-2}$)	Calculated density ($g\,cm^{-2}$)	Inter-particulate spacing (μm)
1	20.2 ± 4.2	20.12	2.586	2.885	6.53 ± 2.1
2	26.1 ± 3.2	0	2.689	2.823	0
3	21.6 ± 2.2	17.5	2.574	2.8802	7.214 ± 1.9

microscope. Fine microstructural features were revealed by transmission electron microscopy (TEM). Samples for TEM observation were prepared from discs of 3 mm diameter, thinned by electrolytic polishing in a single-jet electropolishing unit using 1:3 mixture of nitric acid in methanol maintained at a temperature of −20 °C (263 K) and at an applied potential difference of 15 V. The polished foils were examined in a Phillips CM 20 transmission electron microscope at an operating voltage of 100 kV.

The volume fraction of ceramic particulates (SiC_p) was determined using the chemical dissolution method. This method involved: (a) measuring the mass of composite samples, then (b) dissolving the samples in 30% hydrochloric acid, followed by (c) filtering to separate the ceramic particulates. The fine particulates were then dried and the weight fraction determined. The weight fraction was converted to volume fraction, $V_{fSiC}(\%)$, using the equation

$$V_{fSiC} = \frac{\text{wt \% SiC}/\rho_{SiC}}{\text{wt \% SiC}/\rho_{SiC} + \text{wt \% matrix}/\rho_{matrix}} \quad (1)$$

where ρ_{SiC} is the density of silicon carbide, and ρ_{matrix} is the density of the aluminium alloy matrix.

The inter-particle distance was obtained using the equation [38]

$$\lambda = (l\,t/f)^{1/2} \quad (2)$$

where λ is the interparticle spacing, lt is the cross-sectional area of the particulate reinforcement, and f is the volume fraction of reinforcement obtained from chemical analysis.

Cylindrical tensile samples were machined from the unreinforced matrix alloy 2519 and the 2519/SiC_p metal-matrix composite, such that the longitudinal direction was parallel to the extrusion direction. Thus, the gross fracture plane was perpendicular to the extrusion direction. Uniaxial smooth-bar tensile properties were determined in accordance to ASTM Standard E8-81. The specimens were deformed to failure in an Instron (Model 1125) structural test machine at a constant crosshead speed of 0.0254 cm min^{-1}. The tests were conducted at ambient temperature and in laboratory air environment. Fracture surfaces of the deformed samples were examined in a scanning electron microscope to determine the fracture mode and to characterize the fine-scale features on the quasi-static fracture surface.

3. Results

3.1. Initial microstructure

The spray-atomized and co-deposited preform, henceforth referred to as the spray-processed material, had a typical peak shape geometry with a height of 90 mm and a diameter of 140 mm. Microstructural analysis was conducted on the spray-processed specimens taken from the central region of the perform.

Optical microscopy examination of the unreinforced AA2519 matrix and the silicon carbide particulate (defined as SiC_p)-reinforced AA2519 metal matrix revealed the presence of an equiaxed grain morphology, Fig. 2. The grain size of the particulate-reinforced metal matrix is observed to be considerably smaller than that of the unreinforced counterpart. Both the unreinforced and reinforced materials revealed the presence of fine particles at and along the grain boundaries and even within the grain for the spray-processed composite material. The results of grain-size measurements are summarized in Table II. The distribution of the particulate reinforcements in the ductile aluminium alloy matrix is significantly improved following extrusion at high temperature. Fig. 3 shows a uniform distribution of the SiC_p in the extruded composite.

The results of density measurements revealed a density of 2.689 $g\,cm^{-3}$ for the unreinforced AA2519, and a density of 2.586 $g\,cm^{-3}$ for samples taken from experiments 1 and 3 of 2519/SiC_p. The results of the chemical (acid) dissolution study revealed the volume percentages of SiC particulates in the as-spray deposited material to be approximately 20.12% for experiment 1 and 17.5% for experiment 3. The interparticle spacing was estimated using the formula suggested by Nardone and Prewo [45] for discontinuous reinforcements in a ductile matrix. The results of the computed interparticle spacings, λ, are summarized in Table II.

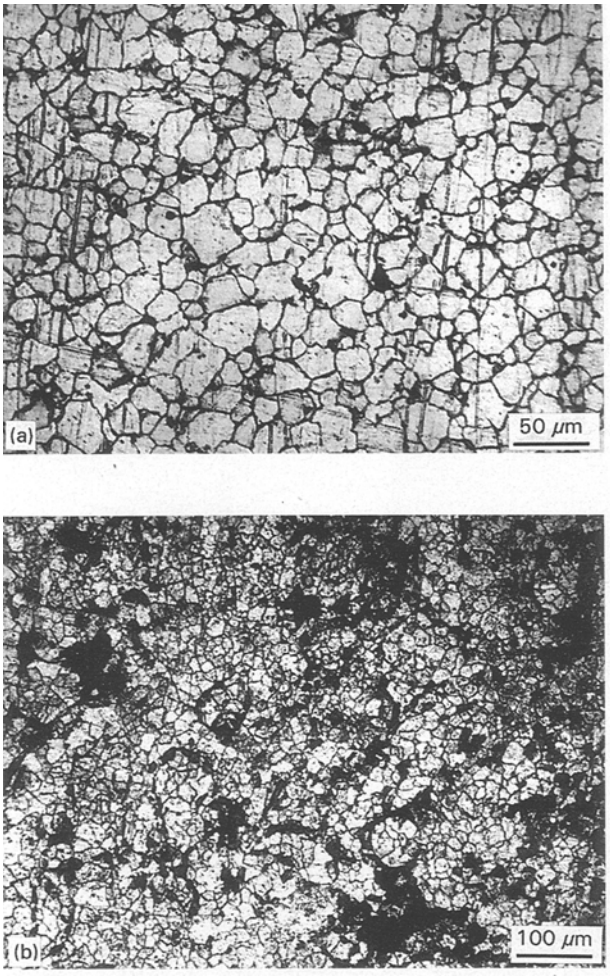

Figure 2 Optical micrographs showing (a) an equiaxed grain morphology in aluminium alloy 2519 processed by spray deposition, and (b) fine microstructure in SiC-reinforced aluminium alloy 2519 processed by spray deposition.

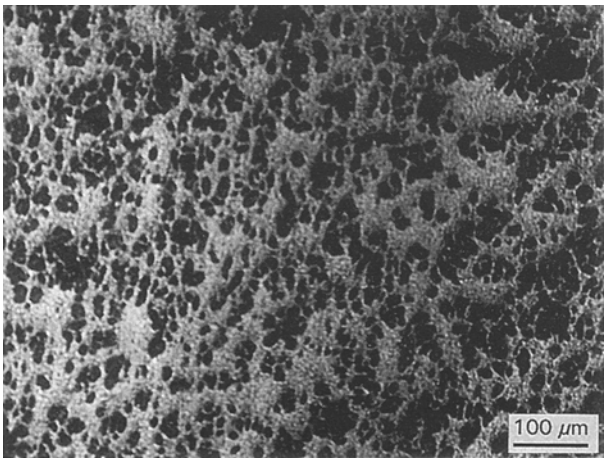

Figure 3 Optical micrograph showing uniform distribution of the SiC particulates following extrusion of the aluminium alloy composite.

To provide an insight into the interaction between the liquid droplets of the melt and the SiC particulates, the morphology of a solidified droplet is shown in Fig. 4. Preferential clustering or agglomeration of the particulates (SiC_p) occurs at and along the droplet boundaries, with few particulates randomly distributed within the interior of the droplet. Fig. 4b is an optical micrograph of an over-sprayed droplet and

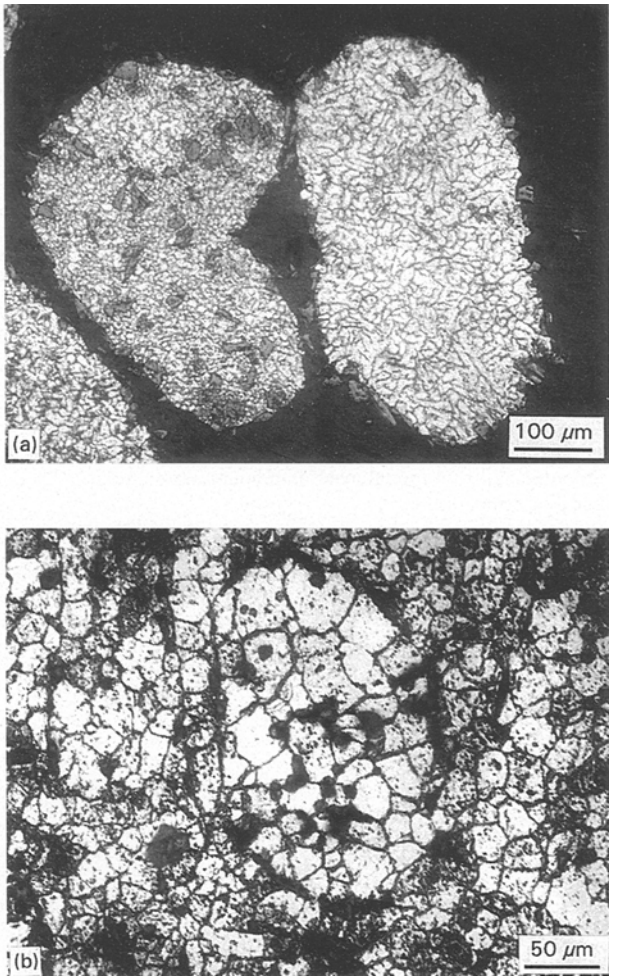

Figure 4 Optical micrographs (a) of an over-spray droplet showing the microstructure resulting from SiC injection into the droplet, and (b) showing typical SiC_p distribution within a droplet.

reveals a remarkable difference resulting from SiC_p injection into the droplet. A dramatic difference in the grain size was also observed between those droplets having the particulate reinforcement and those without the particulate reinforcement.

3.2. Grain-growth behaviour

Fig. 5 exemplifies the variation of grain size with time, to rationalize the effect of SiC_p on grain growth. The grain size of the particulate-reinforced metal matrix is smaller when compared with the unreinforced matrix material, both materials annealed at 450 °C. The presence of SiC_p significantly decreases the growth of grains with time. The microstructure of the as-spray-processed monolithic alloy and the 2519/SiC_p composite essentially consisted of equiaxed grains.

Table II summarizes quantitative image analysis and chemical analysis conducted on the as-spray-processed specimens. The grain size of the SiC_p-reinforced 2519 matrix is about 30% smaller than that of the unreinforced material.

3.3. Ageing studies

The results of ageing studies conducted on both the reinforced and unreinforced alloy 2519 are shown in

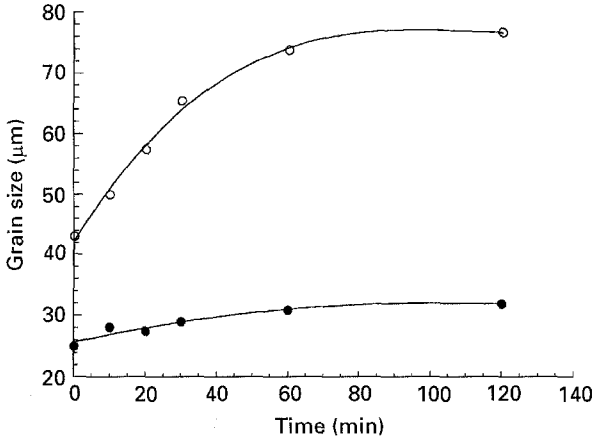

Figure 5 Variation of grain size with time for both the (●) SiC-reinforced and (○) unreinforced aluminium alloy 2519, at 733 K annealing temperature.

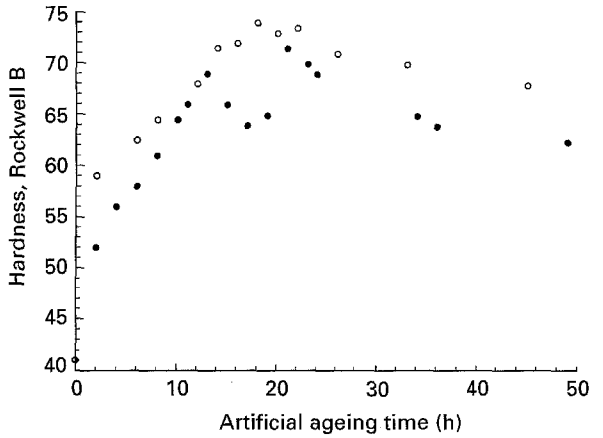

Figure 6 Variation of hardness with ageing time for the (●) SiC reinforced and (○) unreinforced aluminium alloy 2519 materials, at 435 K ageing temperature.

Fig. 6. This figure shows the variation of hardness with ageing time for both materials aged at 163 °C. In the case of the 2519/SiC_p composite, results reveal two well-defined peaks, the first at 14 h and the second at 22 h, in the hardness curve. However, the unreinforced matrix exhibits only one well-defined peak at 20 h. It is interesting to note that the as-quenched hardness achieved by the 2519/SiC_p MMC is lower than the unreinforced counterpart. However, it is observed that the presence of fine silicon carbide particulates accelerates the ageing kinetics, that is, the time required to reach peak strength.

3.4. Electron microscopy observation

Transmission electron microscopy (TEM) observations of the as-spray-processed particulate-reinforced AA2519 matrix, reveals regions of higher dislocation density at and around the SiC_p/matrix interface (Fig. 7). It was also observed that growth of the recrystallized grains occurred at the expense of the subgrains (Fig. 8). The electron microscopy studies were conducted on both the unreinforced and reinforced materials, in the T6 peak-aged condition, to obtain an understanding of reinforcement influence on precipitation behaviour, their morphology and distribution. Fig. 9a

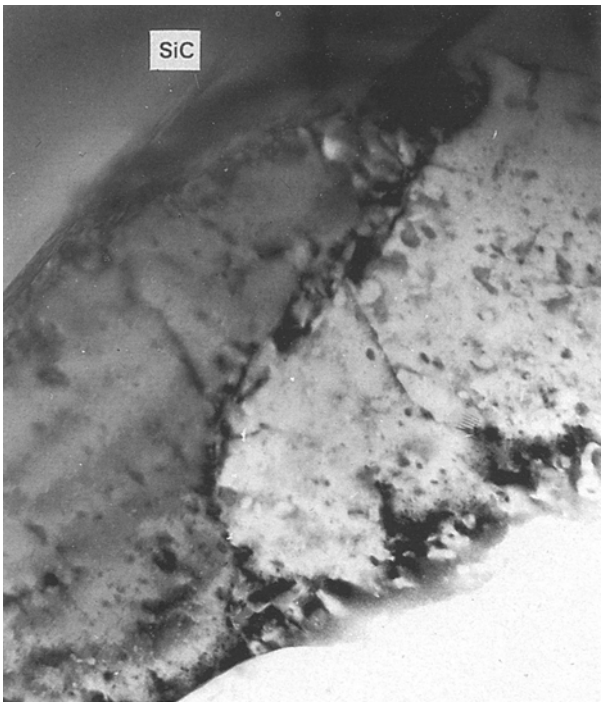

Figure 7 Bright-field transmission electron micrograph showing dislocations along the SiC/matrix interface.

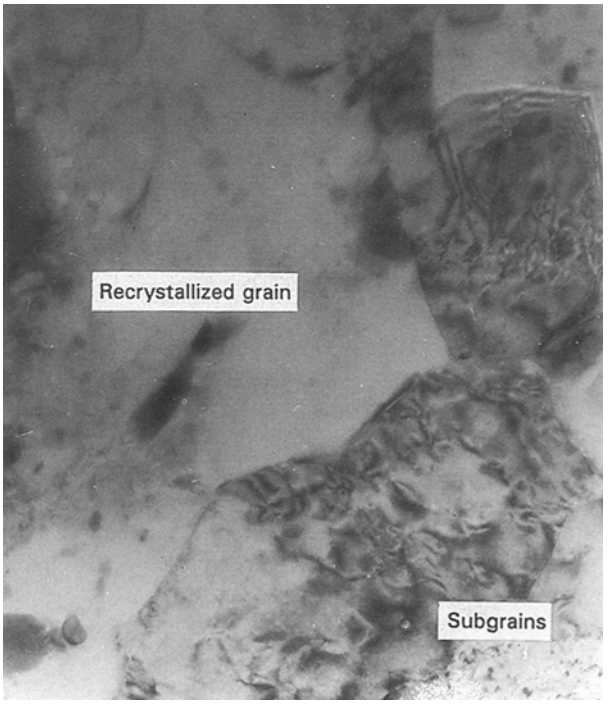

Figure 8 Bright-field transmission electron micrograph showing a recrystallized grain growing at the expense of subgrains.

shows the morphology of the copper-rich precipitates in the matrix of the unreinforced material. The Al–Cu precipitates exhibit a fine needle-shape morphology. The corresponding selected-area diffraction pattern taken from the same region (Fig. 9b) reveals the precipitates to lie along the [1 0 0] habit plane with an orientation relationship $\langle 1\,2\,0\rangle_{ppt} \| \langle 1\,0\,0\rangle_{matrix}$. Based on precipitate morphology and diffraction analysis, these precipitates are the Al_2Cu (θ′) [46, 47].

In the 2519/SiC_p composite, an additional phase was distinctly observed beside the θ′ (Al_2Cu) precipitate.

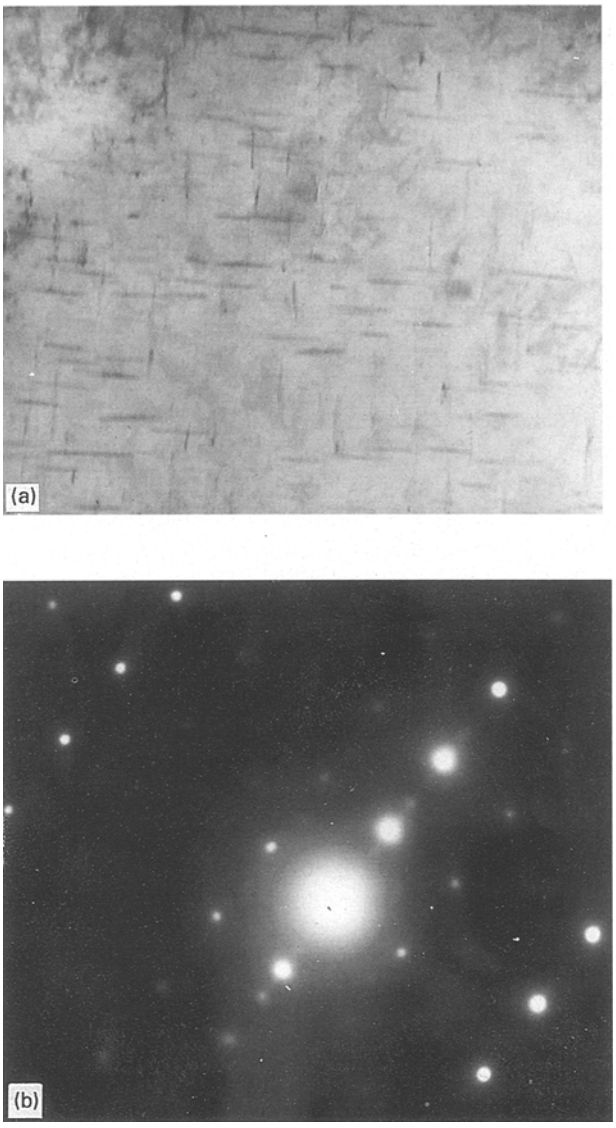

Figure 9 (a) Bright-field transmission electron micrograph showing the needle-shaped Al–Cu precipitates, in the T6 condition, of the unreinforced matrix material. (b) Corresponding selected-area diffraction pattern taken from the same region.

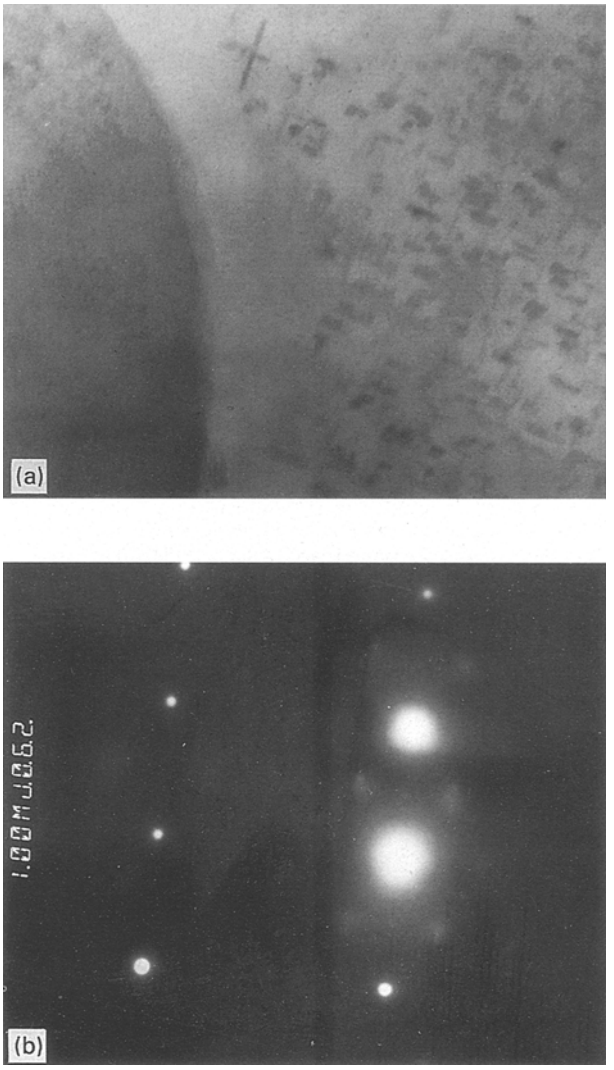

Figure 10 (a) Bright-field transmission electron micrograph showing the morphology of the major strengthening precipitates and the PFZ at the interface, in the aluminium alloy 2519/SiC_p composite. (b) Corresponding selected-area diffraction pattern taken from the same region indicating precipitate orientation.

The diffraction pattern of this phase, which when indexed, gives a lattice parameter of 0.5899 nm. The composition of this phase is most likely Al_7Cu_2Fe. The θ′ precipitates in the Al/SiC_p MMC appeared to have a needle-shape morphology but were finer, shorter in size and uniformly distributed when compared to the precipitates in the unreinforced matrix material. Moreover, the 2519/SiC_p composite revealed the existence of a narrow precipitate-free zone (PFZ) at and along the interfaces of the SiC_p and the matrix (Fig. 10a). The width of the precipitate-free zone, in the T6 peak-age condition, was around 0.5 μm.

3.5. Tensile properties

The results of ambient temperature tensile properties of the SiC_p reinforced and unreinforced alloy 2519 are summarized in Table III. Duplicate tests were done for each condition and no significant variation between the pairs of samples was observed. The 2519/SiC_p composite exhibits lower strength and ductility when compared to the unreinforced matrix counterpart. In both the underaged (UA) and peak aged (PA) conditions, the yield strength (YS) and ultimate tensile strength (UTS) of the MMCs are lower than that of the unreinforced counterpart (2519), in the T6 condition. In the peak-aged condition, the decrease in tensile strength is as high as 28%, while the decrease in yield strength is only marginal. However, the peak-aged material shows an improvement in strength over the under-aged counterpart. The ductility decreased from 7.2% for the unreinforced material to 3.9% for the underaged 2519/SiC_p composite and 1.8% for the peak aged 2519/SiC_p composite.

TABLE III Tensile test properties

		Yield stress (0.2%) (MPa)	UTS (MPa)	Elongation (%)
Al–2519	(peak aged)	311 ± 76.3	444 ± 7	7.2 ± 0.65
Al-2519/SiC_p	(under aged)	256 ± 5.1	297 ± 6.4	3.9 ± 0.31
Al–2519/SiC_p	(peak aged)	304 ± 9.3	320 ± 21.2	1.8 ± 0.51

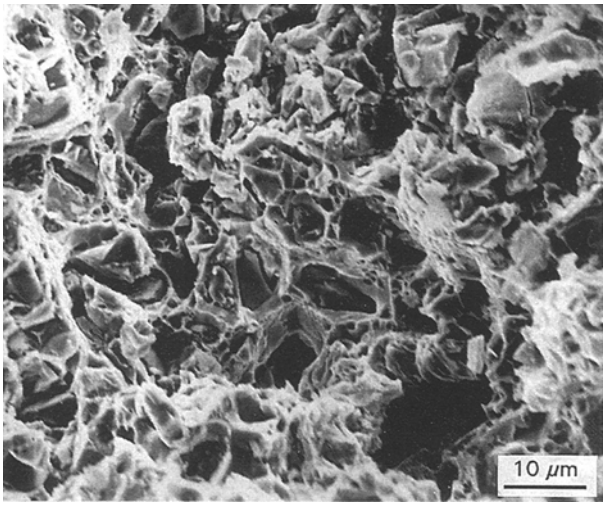

Figure 11 Scanning electron micrograph showing overall morphology of the tensile fracture surface of the 2519/SiC_p composite.

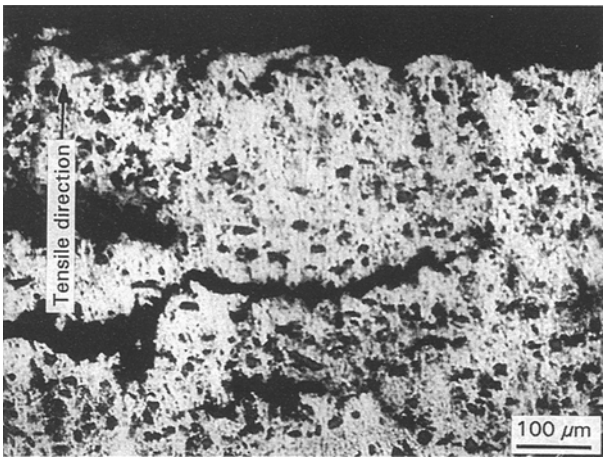

Figure 12 Optical micrograph of the vertical section showing cracks in the 2519/SiC_p composite.

3.6. Tensile fracture behaviour

Fig. 11 is a representative fractograph showing morphology of the tensile fracture surface of the peak-aged 2519/SiC_p composite sample. The tensile fracture surface revealed combinations of (a) decohesion of SiC particulates from the matrix, (b) particulate debonding, (c) cleavage rupture, and (d) ductile tearing.

High-magnification observations of the fracture surface revealed plastic deformation at and along the interfaces between the SiC_p and the aluminium alloy matrix. Adjacent to the plastic zone, the fracture surface revealed the presence of cleavage-like features. The overload region comprised ductile dimples and tearing, features reminiscent of ductile failure. Image analysis conducted on the tensile fracture surface revealed the SiC particulate surface to be 8.0%, the cleavage area at 42% and the local plastic region at 56%, indicative of the limited ductility of the composite.

Metallographic observations along the direction of the major stress axis revealed the occurrence of cracking in the longitudinal direction and perpendicular to the fracture surface (Fig. 12). The cracks were observed to have initiated at the larger particulates and propagated along regions of particulate agglomeration. In fact, a large number of microcracks were observed to have initiated at the particulate clusters.

4. Discussion

4.1. Microstructure of the spray-processed composite

A fairly high volume fraction of SiC_p reinforcement in the 2519 matrix was achieved by the spray atomization and co-deposition technique. The symmetrically arranged four injectors are believed to be largely responsible for successful distribution of the SiC particulates in the metal matrix. The injector configuration delivers a high amount of the SiC_p ($130\ g\ s^{-1}$) into the molten metal spray at a fairly low injecting pressure (25 p.s.i. (1 p.s.i. $= 7.0307 \times 10^2\ kg\ m^{-2}$)). This facilitates an effective mixture of the particulate (SiC_p) with the metal matrix. At the same time, the injected particulates are uniformly distributed. As shown in Fig. 2, the fine SiC_p are uniformly distributed within the aluminium alloy metal matrix and harmonize well with the fine grain size of the as-spray-deposited material. Subsequent extrusion of the as-spray deposit aids in refining and enhancing particulate distribution, resulting in a refined final microstructure of the 2519/SiC_p composite.

The spray-deposited 2519/SiC_p composite had an equiaxed grain morphology. This observation conforms well with results obtained by other investigators [42, 50–55]. The test data also indicate that variation in atomization pressure failed to induce any appreciable change in grain size, which is observed by comparison of the grain size of experiments 1 and 3. On the other hand, the presence of the particulate reinforcement in the spray does effectively reduce the grain size of the as-sprayed deposit by as much as 30%. A quantitative relationship between reinforcement volume fraction and grain size was not done in this study. However, it is observed that an increase in particulate volume fraction effectively decreases the grain size of the as-spray-deposited material. The results convincingly show that the grain size of the unreinforced material is higher than that of the composite counterpart.

In an earlier study, Gupta *et al.* [41] showed that the optimum injector distance should be at a position where at least 20% of the mean droplet size (50 μm) had solidified. The thermal history of droplets of the molten metal during flight can be considered as comprising of three regions: (a) cooling of the fully liquid droplets; (b) the cooling of the mushy droplet; and (c) the cooling of the fully solid particle. The cooling rate progressively decreases once solidification starts, owing to the release of latent heat of solidification. Prior numerical studies [54–57] have shown that the atomized spray virtually consists of a combination of large-sized liquid and semi-liquid droplets and a considerable amount of solidified or near-solidified small droplets which have a relatively higher cooling rate than the larger droplets. When the reinforcing particulates impact with the droplets of the molten metal at the correct angle, the following events occur either independently or conjointly.

(a) The large-size droplets remain in the liquid and the surface temperature is fairly high to retain a lower droplet surface tension. As a result, particulates can easily penetrate into the droplets of the molten metal. Direct evidence can be found in Fig. 4, which shows SiC particulate penetration into the centre of the droplet of the molten metal.

(b) For the partially solidified droplets, the solidification kinetics starts from the droplet surface in the form of dendrites. The unsolidified part may have a slightly higher temperature due to the recalescense effect. Consequently, the surface tension decreases, which makes it easy for the impacting ceramic (SiC) particulates to penetrate into the partially solidified droplet. However, the solid dendrite arms will prevent any further penetration of the impacting SiC particulate. This provides an appealing rationale for the preferential accumulation of the SiC particulates at and along the droplet boundaries (Fig. 4).

(c) The completely solidified droplets will have an elastic impact with the injecting SiC particulate. This type of droplet will exert an influence on the distribution of SiC particulate reinforcement only when the volume fraction of solidified droplets is high.

A mixture of co-injecting reinforcement particulate with molten-metal droplets will tend to decrease the enthalpy of the droplet during flight, because of thermal energy transfer between the reinforcing SiC particulates and droplets of the molten metal. Consequently, the droplet temperature decreases due to the mixing effect. The total enthalpy drop in the droplet due to the presence of the particulate reinforcement can be effectively described by the relationship

$$\Delta H = AM_s(\text{wt \% SiC}) \int_{T_o}^{T} C_p \, dt \qquad (3)$$

where T is the balance temperature, T_o the initial temperature of the SiC particulate, C_p the specific heat of SiC, M_s the mass of the droplet, wt % SiC is the weight percentage of the particulate, and A the coefficient of mixing effectiveness. This expression shows that overall enthalpy loss is proportional to the amount of particulate reinforcement. However, the thermal energy loss is limited to the larger-sized droplets which have a higher probability of contact with the SiC particulate. Numerical analyses have convincingly shown that droplet temperature distribution is a strong function of droplet size at a concerned elevation [33, 53]. During the flight stage, the decrease of droplet temperature is governed by synergistic and competing influences of surface conduction and radiation. The smaller sized droplets have a higher surface-to-volume ratio, which leads to a higher heat loss during droplet flight. This means that the smaller droplets have a higher cooling rate than the larger droplets. Consequently, the higher cooling rate results in a higher solidification for the smaller droplets than for the larger-sized droplets. Moreover, the presence of the injected particulate partially compensates for the uneven cooling rate among the different size droplets. This is achieved by decreasing the temperature of the larger droplets, which directly translates to a higher solidification rate for the larger droplets. Finally, a higher cooling rate in the overall spray will result in a smaller grain size for the final deposit compared with the unreinforced matrix material. This explanation conforms well with present experimental findings, shown in Fig. 5b, which reveal the grain size of the 2519/SiC_p composite to be considerably smaller than the grain size of the unreinforced matrix alloy 2519 deposit made under identical conditions. It can also be anticipated that increasing the volume fraction of particulate reinforcement will further decrease the grain size of the final product. However, because the smaller liquid droplets are not appreciably affected by mixture with the SiC particulate reinforcement during flight, this prediction has its limitations.

The presence of particulate reinforcement enhances grain nucleation by the following intrinsic mechanisms [42, 43] :

(a) The particulate exists as a heterogeneous nucleation centre and fosters the nucleation rate prior to its impact on to the substrate;

(b) fragmentation of dendrite arms is a mechanism responsible for nucleation in the final stage.

The solidified part is present in the form of dendrites in the droplet. On the other hand, the thermal expansion coefficient of the SiC-particulate reinforcement and the ductile aluminium alloy are different. For example, the thermal expansion coefficient of SiC is $5.7 \times 10^{-6}\ K^{-1}$, while that of the aluminium matrix is $25.3 \times 10^{-6}\ K^{-1}$. The significant difference tends to induce local stress concentration in the region of the SiC_p/2519 interface. This makes the dendrites relatively brittle. Consequently, fragmentation of the brittle dendrites occurs on their impact with the substrate at high speed. This mechanism enhances the nucleation kinetics during final solidification. Moreover, the presence of SiC_p further enhances grain growth. At this stage, the cooling rate is relatively decreased and grain growth is crucial for controlling grain size of the final deposit. The experimental results, shown in Fig. 6, reveal that the presence of SiC_p retards grain-growth rate at elevated temperatures. Gupta *et al.* [41, 48] reported a similar observation of SiC_p-reinforced aluminium-lithium alloy. The SiC particulates act as effective barriers for grain-boundary migration. It has been suggested that the dislocation concentration at the interface region may be a direct evidence of the particulate-retarding grain-boundary migration [58]. Generation of dislocations is an energy-consuming process which contributes to retarding grain-boundary migration [59].

Fig. 4 reveals that extrusion processing aids in eliminating the pores in the Al–2519/SiC_p composite. This is well supported by density measurements listed in Table II. In the as-deposited material the pores were associated with droplet boundaries where clustering of the reinforcing SiC particulates exits. Considering the processing variables used for the three independent experiments (Table I), porosity is influenced and/or affected by competing influences of atomization pressure and particulate flow rate. It is most likely, as observed from density measurements, that the presence of the SiC particulate induces or promotes

porosity in the as-sprayed deposit. Our experimental results support the view that interstitial porosity among the partially solidified droplets is the dominant mechanism to form pores. The rationale for the presence of SiC particulates at and along the boundaries can be attributed to collision of the liquid droplets with the ceramic particulate. On the other hand, any absorbed gas by the particulate is released at high temperatures and is an alternative explanation for the high porosity associated with the discontinuous reinforcement.

4.2. Precipitation during ageing

Hardness measurements and transmission electron microscopy observations revealed that the presence of SiC_p in the ductile aluminium alloy matrix influences the precipitation kinetics. For the SiC-reinforced AA-2519 composite, an additional phase having a cubic morphology was found beside the dominant strengthening Al–Cu (θ′) precipitate. Furthermore, the Al–Cu precipitate grows on the {1 1 4} habit plane rather than the {1 0 0} plane in the unreinforced AA-2519. A plausible reason for the change in habit plane is the internal stress in the matrix induced by intrinsic differences in the coefficient of thermal expansion between the SiC reinforcement and the aluminium alloy matrix. The significant difference in thermal expansion coefficients tends to induce compressive stresses in the matrix during quenching following solution heat treatment. The internal stresses enhance and promote precipitation of the θ′ precipitate on a different habit plane.

Microstructural observations also revealed that at and along the interface region the dislocation density was fairly low following extrusion at high temperature. A fairly well-developed recrystallized structure had formed. This conforms well with the findings documented by other investigators [60]. In this earlier study, the existence of a dislocation-free zone along the SiC interface was reported for AA-6061/SiC_p composite. Also, a precipitate-free zone along the SiC boundary was observed for the peak aged (PA) condition. It is generally believed that the large difference in the coefficient of thermal expansion between the ceramic particle (SiC_p) reinforcement and the matrix induces considerable amounts of dislocations at and along the interfaces. The density of dislocation build-up depends on the competing influences of several processing parameters such as temperature, extrusion ratio, and extrusion speed. In this study, a recrystallized microstructure was evident following extrusion. Formation of subgrains and recrystallization are structure-recovery processes which develop at the expense of dislocation density. This is an appealing rationale for the lower dislocation density along the grain-boundary regions.

Regarding the formation and presence of a precipitate-free zone at and along the SiC interfaces, there is no convincing explanation to offer at this time. However, based on the intrinsic micromechanisms responsible for PFZ formation and considering the lack of reaction products at the interface, the vacancy-depleted model may be the explanation for its formation [61, 62]. At high temperatures, the interface is a potential sink for the defects such as dislocations and vacancies, which partially annihilate each other by diffusion. Consequently, defect concentration both at and along the interface region is not adequate enough to promote precipitate nucleation.

4.3. Mechanical behaviour

Several investigators have found and documented that reinforced-particulate cavitation is a primary mechanism responsible for failure in the MMCs [63–65]. This mechanism assumes that crack initiation occurs at the fractured particulates or clusters of particulates. Under the influence of an applied load, these cracks propagate into the matrix and grow. This phenomena has been observed on the fracture surfaces by scanning electron microscopy (SEM) and by optical metallographic observation of the vertical section. However, quantitative image-analysis results convincingly show that the exposed SiC surface area is only 7.5% on the fracture surface, far less than the volume fraction used (23%). Also, decohesion occurred at the SiC–2519 interface, although it was difficult to identify these sites quantitatively. The intrinsic difficulty suggests that the particulate decohesion model is not the dominant mechanism contributing to failure of this 2519/SiC_p metal-matrix composite.

An examination of the fracture surface revealed considerable amount of SiC particulates to be pulled out from the matrix, which is quite typical in the case of particulate–matrix debonding. Although no reaction products were found to exist at the SiC_p–2519 interface, it is most unlikely that the interface is a simple mechanical joint. Because mechanical joining cannot fully transfer the load, all of the SiC particulates should separate from the matrix prior to fracture. The presence of a low volume fraction of SiC_p on the fracture surface fails to support the above hypothesis. On the other hand, a slight decrease in yield strength is an indication for declining the assumption of a simple mechanically joint interface. If the law of mixtures can be used to describe the tensile strength of the metal–ceramic particulate composite, then the total strength of the MMC should be

$$\sigma_{total} = \alpha\sigma_{matrix} + \beta\sigma_{SiC} + \mu\sigma_{interface} \quad (4)$$

where α, β, μ are the corresponding surface fractions at a cross-section.

It is clear that at the interface both the particulate reinforcement and the metal matrix contribute to total strength. This is a reasonable approach, at least before yielding. If a simple mechanical joint interface is assumed, implying that the applied far-field tensile load can be transferred to the particulate reinforcement, the 23 vol % SiC_p should contribute to the yield strength. This assumption is apparently not true based on the results obtained. On the other hand, if bonding of the reinforcement with the matrix is perfect, such that the reinforcement can take all of the applied load, the expected yield strength should be higher than the measured value. However, the presence of fractured

SiC particulates on the tensile fracture surface provides a convincing rationale as to why the volume fraction of SiC reinforcement is not capable of taking the full tensile load. The fractured SiC particulates function as cavities in the material. Consequently, the effective load-resisting area is decreased. The loss in strength is partially compensated for by the particulate reinforcement.

Examination of the fracture surface at high magnification reveals the presence of plastic deformation region around the SiC particulates. The plastic deformation was concentrated at and along the particulate boundaries. Under the influence of a far-field tensile stress, the precipitate-free zone (PFZ) will yield first on account of its lower strength. Consequently, the dislocations move rapidly into the interface of the precipitate- matrix and induce crack initiation at the interface. Continued application of the far-field stress causes the crack to extend into the matrix. As a result, the overall ductility of the composite matrix is degraded. Shallow equiaxed dimples and microvoids were observed on the tensile fracture surface, features reminiscent of ductile failure.

5. Conclusions

Based on the results obtained in this study, the following are the key conclusions.

1. A fairly high volume fraction of ceramic particle reinforcement (SiC) in AA-2519 was achieved using the spray-atomization and co-deposition processing technique.

2. The presence of SiC particulates significantly affects the microstructures of the 2519/SiC_p composite by impinging into droplets of the molten metal. The intrinsic mechanisms include synergistic and competing influences of an increase in droplet cooling rate resulting in promoting nucleation, and retarding grain-boundary migration and suppressing grain growth.

3. The presence of SiC particulates in aluminium alloy 2519 matrix alters the precipitation kinetics during artificial ageing. A cubic phase was found in the peak-aged composite besides the primary Al–Cu precipitates, θ'. Also, a precipitate-free zone (PFZ) was observed at and along the interfaces between the carbide particulate and the metal matrix. Further work is necessary to understand the precipitation behaviour in this aluminium alloy composite.

4. Inferior tensile strength and ductility of the composite are attributed primarily to pre-existing cavitation due to the fractured particulates and particulate clusters. However, the precipitate-free zone promotes enhanced crack nucleation at the interface and this also contributes to the inferior ductility and fracture resistance of the composite.

Acknowledgements

E. J. L thanks Dr Ed Chen, Army Research Office (Grant No. DAAL03-92-G-0181), for financial support and encouragement. T.S.S thanks the ALCOA Technical Center for providing partial support during the course of the preparation of this manuscript.

References

1. S. DERMARKAR, *Metals Mater.* **2** (1986) 144.
2. S. V. NAIR, J. K. TIEN and R.C. BATES, *Int. Metals Rev.* **30** (1985) 275.
3. D. L. McDANELS, *Metall. Trans.* **16A** (1985) 1105.
4. S. NOROSE, T. SASADA and M. OKABE, in "28th Japan Congress on Materials Research" (1985) pp. 231–40.
5. D. L. DAVIDSON, "Micromechanisms of Fatigue Crack Growth and Fracture Toughness in MMCs", South West Research Institute Technical Report to Office of Naval Research (1987).
6. JIAN KU SHANG and R. O. RITCHIE, *Metall. Trans.* **20A** (1989) 897.
7. D. F. HASSON, C. R. CROWE, J. S. AHERN and D. S. COOKE, "Failure Mechanisms in High Performance Materials" (Cambridge University Press, Cambridge, 1985) pp. 147–55.
8. W. L. PHILLIPS, in "Proceedings of the Conference on Composite Materials", edited by B. Noton (Metallurgical Society of AIME, Warrendale, PA, 1978) pp. 567–74.
9. T. G. NIEH, *Metall. Trans.* **15A** (1984) 139.
10. G. GOULD, in "Proceedings of the Third International Conference on Isostatic Pressing", Vol. 1 (London, 1986).
11. R. J. ARSENAULT, *Mater. Sci. Eng.* **64** (1984) 171.
12. H. J. RACK, *Adv. Mater. Manuf. Process.* **3**(3) (1988) 32.
13. I. A. IBRAHIM, F. A. MOHAMED and E. J. LAVERNIA, *J. Mater. Sci.* **26** (1991) 1137.
14. D. L. DAVIDSON, *Metall. Trans.* **18A** (1987) 2125.
15. S. MANOHARAN and J. J. LEWANDOWSKI, *Acta Metall.* **38** (1990) 489.
16. D. L. DAVIDSON, *Eng. Fract. Mech.* **33** (1989) 965–75.
17. A. P. DIVECHA, S. G. FISHMAN and S. D. KARMARKAR, *J. Metals* **33**(9) (1981) 12.
18. W. A. LOGSDON and P. K. LIAW, *Eng. Fract. Mech.* **24** (1986) 737.
19. D. L. DAVIDSON, *Metall. Trans.* **22A** (1991) 97.
20. T. S. SRIVATSAN, I. A. IBRAHIM, F. A. MOHAMED and E. J. LAVERNIA, *J. Mater. Sci.* **27** (1992) 5965.
21. XD™, US Pat. 4710–348 (1990).
22. A. R. C. WESTWOOD, *Metall. Trans.* **19A** (1988) 749.
23. L. CHRISTODOULOU, P. A. PARRISH and C. R. CROWE, in "High Temperature/High Performance Composites", Materials Research Society Symposium Proceedings, Vol. 120, edited by F. D. Lemkey, S. G. Fishman, A. G. Evans and J. R. Strife (Materials Research Society, Pittsburgh, PA, 1988) pp. 29–39.
24. L. WANG and R. J. ARSENAULT, *Metall. Trans.* **22A** (1991) 3013.
25. D. D. VVEDENSKY, M. E. EBERHART, L. CHRISTODOULOU, S. CRAMPIN and J. M. MacLAREN, *Mater. Sci. Eng.* **A126** (1990) 33.
26. D. E. LARSEN, L. CHRISTODOULOU, S. L. KAMPE and P. SADLER, Materials Science and Engineering, A144, 1991, pp. 45–55
27. E. W. LEE, J. COOK, A. KHAN, R. MAHAPATRA and J. WALDMAN, *J. Metals* **43** (1991) 54.
28. A. R. E. SINGER and S. OZBEK, *Powder Metall.* **28**(2) (1985) 72.
29. M. GUPTA, F. A. MOHAMED and E. J. LAVERNIA, *Mater. Manuf. Process.* **5**(2) (1990) 165.
30. *Idem*, **23A** (1992) 831.
31. *Idem, ibid.* **23A** (1992) 845.
32. *Idem, Mater. Sci. Eng.* **144A** (1991) 99.
33. *Idem, Int. J. Rapid Solid.* **6** (1991) 247.
34. M. GUPTA, I. A. IBRAHIM, F. A. MOHAMED and E. J. LAVERNIA, *J. Mater. Sci.* **26** (1991) 6673.
35. E. J. LAVERNIA, *SAMPE Q.* **22** (1991) 2.
36. R. J. PEREZ, J. ZHANG, M. N. GUNGOR and E. J. LAVERNIA, *Metall. Trans.* **24A** (1993) 702.
37. A. R. E. SINGER, *Mater. Sci. Eng.* **135A** (1991) 297.

38. Y. WU and E. J. LAVERNIA, *J. Metals* **43**(8) (1991) 16.
39. T. S. SRIVATSAN and E. J. LAVERNIA, *J. Mater. Sci.* **27** (1992) 5965.
40. J. WHITE, I. R. HUGHES, T. C. WILLIS and R. M. JORDON in "Fourth Int. Conference on Aluminium–Lithium", Paris, 10–12 June 1987.
41. M. GUPTA, F. A. MOHAMED and E. J. LAVERNIA, in "Proceedings of the International Symposium on Processing and Characterization of Metal-Matrix Composites", edited by H. Mostaghaci (Pergamon Press, London, 1989) pp. 236–46.
42. M. GUPTA, J. JUAREZ-ISLAS, F. A. MOHAMED and E. J. LAVERNIA, *Metall. Trans.* **23B** (1992) 719.
43. E. J. LAVERNIA, *Int. J. Rapid Solid.* **5** (1989) 47.
44. X. LIANG, J. C. EARTHMAN and E. J. LAVERNIA, *Acta Metall. Mater.* **44** (1992) 3003.
45. V. C. NARDONE and K. W. PREWO, *Scripta Metall.* **20** (1986) 43.
46. J. WHITE, I. G. PALMER, I. R. HUGHES and S. A. COURT, in "Aluminium–Lithium Alloys V", Vol. 3 (edited by E. A. Starke Jr and T. H. Sanders Jr (Materials and Component Engineering, 1989) pp. 1635–45.
47. K. A. KOJIMA, R. E. LEWIS and M. J. KAUFMAN, *ibid.*, Vol. **1**, pp. 85–90.
48. T. S. SRIVASTSAN, M. GUPTA, F. A. MOHAMED and E. J. LAVERNIA, *Aluminium* **68** (1992) 145.
49. M. RUHR, E. J. LAVERNIA and J. BARAM, *Metall. Trans.* **21A** (1990) 1785.
50. R. H. BRICKNELL, *ibid.* **17A** (1986) 583.
51. S. ANNAVARAPU, D. APELIAN and A. LAWLEY, *Metall Trans.* **19A** (1988) 3077.
52. E. J. LAVERNIA, E. GUTIERREZ, J. SZEKELEY and N. J. GRANT, *Progr. Powder Metall.* **43** (1987) 683.
53. E. GUTIERREZ, E. J. LAVERNIA, G. TRAPAGA, J. SZEKELEY and N. J. GRANT, *Metall Trans.* **20A** (1989) 71.
54. E. GUTIERREZ, E. J. LAVERNIA, G. TRAPAGA and J. SZEKELY, *Int. J. Rapid Solid.* **4** (1988) 125.
55. E. J. LAVERNIA, E. GUTIERREZ, J. SZEKELY and N. J. GRANT, *ibid.* **4** (1988) 89.
56. X. LIANG and E. J. LAVERNIA, *Mater. Sci. Eng. A* (1993) in press.
57. E. J. LAVERNIA and N. J. GRANT, *Int. J. Rapid Solid.* **2**, (1986) 93.
58. M. GUPTA, T. S. SRIVATSAN F. A. MOHAMED and E. J. LAVERNIA, *J. Mater. Sci.* **28** (1993) p. 2245.
59. J. ZHANG, R. J. PEREZ and E. J. LAVERNIA, *ibid.* **28** (1993) 835.
60. Z. ZHOU, S. SONG and Y. XU, *Mater. Sci. Eng.* **A132** (1991) 83.
61. N. RYUM, *Acta Metall.* **19** (1969) 921.
62. T. S. SRIVATSAN and E. J. LAVERNIA, *J. Mater. Sci.* **26** (1991) 940.
63. T. S. SRIVATSAN and R. AURADKAR, *Int. J. Fatigue* **14** (1993) 355.
64. T. S. SRIVATSAN, R. AURADKAR, J. M. PANCHAL and A. PRAKASH, *Compos. Eng. Int. J.* **3** (1993) 329.
65. D. J. LLOYD, *Acta Metall. Mater.* **39** (1991) 59.

Received 23 April 1993
and accepted 15 March 1995